A new analytic equation of state for liquid water

C. A. Jeffery and P. H. Austin[a)]
Atmospheric Sciences Programme, #217 Geography, 1984 West Mall, University of British Columbia, Vancouver, British Columbia V6T 1Z2, Canada

(Received 20 May 1998; accepted 1 October 1998)

We develop a new analytical equation of state for water based on the Song, Mason, and Ihm equation of state and Poole *et al.*'s simple model of the free energy of strong tetrahedral hydrogen bonds. Repulsive and attractive forces are modeled using a modification of the Weeks–Chandler–Anderson decomposition of the pair potential, with closed tetrahedral hydrogen bonds contributing both internal energy and entropy to the free energy of water. Strong tetrahedral hydrogen bonds are modeled explicitly using a simplified partition function. The resulting equation of state is 20–30 times more accurate than equivalent simple cubic equations of state over a wide range of pressures (0.1→3000 bar) and temperatures (−34→1200 °C) including the supercooled region. The new equation of state predicts a second liquid–liquid critical point at $p_{C'}=0.954$ kbar, $\rho_{C'}=1.045$ g cm^{-3} and $T_{C'}=228.3$ K. The temperature of this second critical point is above the homogeneous freezing temperature at 1 kbar, thus this region of the phase diagram may be experimentally accessible. The phase diagram also suggests that the homogeneous nucleation temperature above 1.2 kbar may be determined by a phase transition from high-density water to low-density water. © *1999 American Institute of Physics.* [S0021-9606(99)52701-3]

I. INTRODUCTION

Liquid water exhibits a rich variety of anomalous behavior, particularly in the supercooled region. Features of the phase diagram for water such as the density maximum at 4 °C and the minima in the isothermal compressibility K_T and isobaric specific heat C_p are generally acknowledged to be manifestations of the hydrogen bond structure, which at low temperatures produces anomalous behavior in which the internal energy, entropy, and density all decrease with decreasing temperature.[1]

Below we present an analytic equation of state that quantitatively captures this behavior at supercooled temperatures, as well as accurately reproducing the pressure–volume–temperature dependence of water over a broad range of temperatures and pressures. We follow the approach of Poole *et al.*,[2] who showed that the density maximum of water can be qualitatively reproduced by combining the van der Waals equation of state with a simple partition function describing the density dependence of the free energy of hydrogen bonds. To produce quantitative predictions using this approach we extend the work of Poole *et al.* by:

(1) Replacing the van der Waals equation of state by a modified version of the equation of state proposed by Song, Mason, and Ihm.[3]
(2) Modifying the representation of the free energy of hydrogen bonds to localize the temperature range over which strong hydrogen bonds influence the properties of water.

In Sec. II we briefly review the Song, Mason, and Ihm (SMI) equation of state, discuss modifications needed to apply it to water, and evaluate its accuracy over the temperature and pressure range $-34\leqslant T\leqslant 1200$ °C, $0.1\leqslant p\leqslant 3000$ bar. In Sec. III we add the free energy of open hydrogen bonds,[4] and demonstrate the improved predictive power of the equation of state in the supercooled region. Section IV presents the resulting phase diagram showing the second critical point, and Sec. V contains a discussion and conclusions.

II. THE BULK EQUATION OF STATE

A. The Song and Mason equation of state

In a series of articles Song, Mason, Ihm, and colleagues[3,5,6] have derived a simple analytic equation of state for nonpolar fluids. Their starting point is the equation relating pressure p to the pair distribution function $g(r)$:[7]

$$\frac{p}{\rho RT}=1-\frac{2\pi}{3}\frac{\rho}{RT}\int_0^\infty \frac{du(r)}{dr}g(r)r^3dr, \tag{1}$$

where $u(r)$ is the intermolecular pair potential as a function of radial distance r, T the temperature, ρ the density, and R the ideal gas constant. Although the derivation of Eq. (1) assumes pairwise additivity for $u(r)$, many-body effects can still be incorporated through the pair distribution function $g(r)$.

Rearrangement of terms in this equation yields a form in which the second virial coefficient, $B_2(T)$, appears explicitly

$$\frac{p}{\rho RT}=1+B_2\rho+\rho I, \tag{2}$$

with

$$B_2=2\pi\int_0^\infty (1-e^{-\beta u})r^2dr, \tag{3a}$$

$$I=\frac{2\pi}{3}\int_0^\infty f(r)[y(r)-1]r^3dr, \tag{3b}$$

a)Electronic mail: phil@geog.ubc.ca

$$y(r)=e^{\beta u}g(r), \tag{3c}$$

$$f(r)=-\beta\frac{du}{dr}e^{-\beta u}, \tag{3d}$$

$\beta=1/RT$, and the functions $y(r)$ and $f(r)$ are, respectively, the cavity distribution function and the weighting function.[6]

The division of Eq. (1) given in Eq. (2) is motivated by the observation that the attractive forces have a weak dependence on density that can be approximated by the second virial coefficient alone. Thus I, which contains higher order terms in density, is dominated by the repulsive forces. To see explicitly the relative roles played by attraction and repulsion in the integral I, Tao and Mason[8] follow Weeks[9] and split the pair potential $u(r)$ into a part $u_0(r)\leqslant 0$ representing only repulsive forces and a part $u_l(r)\geqslant 0$ representing only attractive forces:

$$u_0(r)=\begin{cases} u(r)+\epsilon, & r<r_m \\ 0, & r>r_m \end{cases}, \tag{4a}$$

$$u_l(r)=\begin{cases} -\epsilon, & r<r_m \\ u(r), & r>r_m \end{cases}, \tag{4b}$$

where $\epsilon>0$ is the depth of the potential well and r_m is the radial distance at which $u(r)$ has its minimum value. They then assume that the dominant contribution to I comes from $r<r_m$ (repulsive forces) and after some manipulation find that

$$I\approx\alpha[G(\sigma^+)-1], \tag{5}$$

where $G(\sigma^+)$ is the pair distribution function of hard spheres at contact, σ^+ is the equivalent hard sphere diameter, and α is a temperature dependent function.

Ihm *et al.*[3] determined that an accurate empirical expression for $G(\sigma^+)$ is

$$G(\sigma^+)=\frac{1}{1-\lambda b\rho}, \tag{6}$$

where b is a temperature dependent function and λ is a constant. The product λb is analogous to the van der Waals excluded volume. Substituting Eq. (6) into Eq. (5) produces

$$I=\alpha\left[\frac{1}{1-\lambda b\rho}-1\right]. \tag{7}$$

Substituting Eq. (7) into Eq. (2) gives the completed Song–Mason–Ihm equation of state:

$$\frac{p}{\rho RT}=1+B_2(T)\rho+\alpha\rho\left[\frac{1}{1-\lambda b\rho}-1\right]. \tag{8}$$

Ihm *et al.*[3] found expressions for the temperature-dependent coefficients α and b in terms of the pair potential $u(r)$. Given these coefficients and B_2, the pair distribution function can then be expressed using Eq. (8) as a function of p, ρ, and T

$$G(b\rho)=\left[\frac{p}{\rho RT}-1+(\alpha-B_2)\rho\right]/\alpha\rho. \tag{9}$$

We can use p-V-T data and Eq. (9) to calculate values of G. From Eq. (6) it can be seen that, if the approximations represented by Eqs. (4) and (5) are accurate, a plot of $1/G(b\rho)$ versus $b\rho$ should produce a straight line with intercept 1 and slope $-\lambda$. Ihm *et al.*[3] have shown that this is the case for many noble gas fluids. As Fig. 1 shows, however, inserting p-V-T data and a B_2 expression appropriate for water into Eq. (9) produces a relatively poor correlation between $1/G$ and the best-fit straight line.

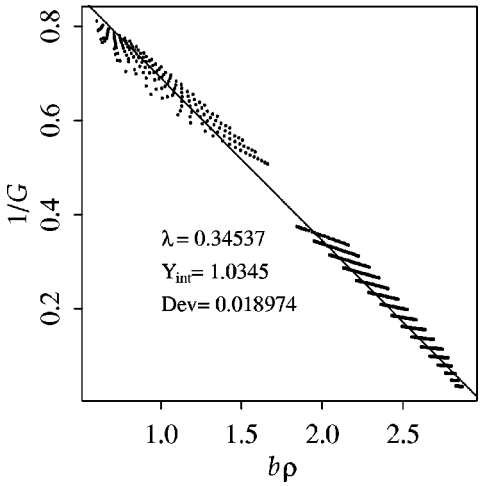

FIG. 1. $1/G$ vs $b\rho$ using Eq. (9), b and α from Tao *et al.* (Ref. 8) and B_2 from Hill and MacMillan (Ref. 45). Also shown is a best fit straight line with slope $-\lambda$, y-intercept Y_{int} and rms deviation, Dev. The 805 p-V-T values are from Haar *et al.* (Ref. 42) in the range $0<T<700$ °C, $0.1<P<1200$ bar, $250<\rho<1015$ kg m^{-3}. The discrete lines in the lower half of the figure represent isotherms spaced 20 °C. Points in the upper half of the figure are above the critical point (Ref. 11).

B. Modifications for a polar fluid

In this section we modify the SMI equation of state so that it can accurately reproduce p-V-T measurements for water. The modifications consist of:

- Changing the partitioning of the pair potential in Eq. (4) so that the attractive and repulsive contributions are clearly separated.
- Evaluating these attractive and repulsive terms using p-V-T measurements and estimates of the hydrogen bond energy and entropy.

In Secs. II B 1–II B 3 we present the the modified equation of state, replacing B_2, α, and $b(T)$ in Eq. (8) with expressions appropriate for a polar fluid. We use Ihm *et al.* strong principle of corresponding states[3] [Eq. (6)] to determine the values for these expressions using the p-V-T data of Fig. 1. A more detailed derivation of the results of this section is available in a separate Appendix.[10]

1. Partitioning the pair potential

To find an alternative to the partitioning given by Eq. (2) that unambiguously separates the attractive and repulsive contributions of the pair potential, we begin by splitting $u(r)$ into its attractive and repulsive parts

$$u(r)=\begin{cases} u_1(r), & r>r_m \\ u_2(r), & r<r_m \end{cases}, \tag{10}$$

where r is the radial coordinate and r_m is the distance to the minimum of the potential.

Inserting Eq. (10) into Eq. (1) yields

$$\frac{p}{\rho RT}=1-\frac{2\pi}{3}\frac{\rho}{RT}\int_{r_m}^{\infty}\frac{du_1}{dr}g(r)r^3dr - \frac{2\pi}{3}\frac{\rho}{RT}\int_{0}^{r_m}\frac{du_2}{dr}g(r)r^3dr = 1-U_A\rho-U_R\rho. \tag{11}$$

where the subscripts A and R refer to attractive and repulsive, respectively.

2. Expressions for U_A and U_R

The attractive contribution U_A in Eq. (11) can be obtained from the free energy due to the attractive part of the potential, $A^{(1)}$, via

$$U_A=\frac{1}{RT}\frac{\partial A^{(1)}}{\partial\rho}, \tag{12}$$

where

$$A^{(1)}=-\frac{\rho}{2}\int_{r_m}^{\infty}u_1(r)g(r)4\pi r^2dr, \tag{13}$$

with $u_1(r)$ defined in Eq. (10).

This expression for the free energy is analogous to the first-order contribution of attractive forces to the free energy of a van der Waals liquid,[7] which we write as

$$A^{(1)}=-a^*\rho, \tag{14}$$

where a^* includes the effect of hydrogen bonds. To estimate a^* note that hydrogen bonds contribute entropy, S_{HB}, as well as energy, ϵ_{HB} to the partition function so that a^* can be written as the sum of these contributions

$$a^*=a+b^*RT, \tag{15a}$$

$$a\approx\epsilon_{\mathrm{HB}}/\rho, \tag{15b}$$

$$b^*\approx S_{\mathrm{HB}}/R\rho. \tag{15c}$$

Substituting Eq. (15a) into Eq. (14) and using Eq. (12) yields

$$U_A=-b^*-a/RT. \tag{16}$$

Thus $U_A\cdot RT\rho$ is simply the van der Waals attractive force $-a_{VW}\rho$ with an additional entropy term $-b^*RT\rho$. Because of the similar role played by a and a_{VW} in this derivation[10] the value of a_{VW} will be used for a below

$$a=a_{VW}=\frac{27R^2T_C^2}{64p_C}=0.5542\ \ \mathrm{Pa\ m^6\ mol^{-2}}, \tag{17}$$

where T_C and p_C are, respectively, the critical temperature and pressure for water.[11]

To evaluate U_R we follow Song and Mason[6] in expanding $y(r)$ in r

$$U_R\approx\alpha G(\sigma^+)=\frac{\alpha}{1-\lambda b\rho}. \tag{18}$$

Substituting Eqs. (16)–(18) into Eq. (11) produces the modified equation of state

$$\frac{p}{\rho RT}=1-b^*\rho-\frac{a_{VW}\rho}{RT}+\frac{\alpha\rho}{1-\lambda b\rho} =1+\left(\alpha-b^*-\frac{a_{VW}}{RT}\right)\rho+\alpha\rho\left[\frac{1}{1-\lambda b\rho}-1\right]. \tag{19}$$

3. Determining b^*, α, and $b(T)$ for liquid water

In the SMI equation of state the temperature dependence of both α and b are determined by integrating over an approximate intermolecular potential for nonpolar fluids. They find that α depends only weakly on temperature for a (12,6) potential; we will treat α as constant when we estimate its value for water below. The excluded volume term b increases with decreasing temperature for a (12,6) potential. This increase will be larger for water than for a nonpolar fluid, because below 4 °C at 1 bar the specific volume increases rapidly with decreasing temperature. We will specify a functional form of $b(T)$ that increases with decreasing T, and use p-V-T data to estimate two undetermined coefficients b_1 and b_2

$$b(T)/v_B=0.25e^{1/(2.3T/T_B+0.5)}-b_1e^{2.3T/T_B}+b_2. \tag{20}$$

We show the fitted form of Eq. (20) in Sec. III B below.

Given Eq. (19), the new expression for $G(b\rho)$ is

$$G(b\rho)=1/(1-\lambda b\rho) \tag{21a}$$

$$=1+\left[\frac{p}{\rho RT}-1-\left(\alpha-b^*-\frac{a_{VW}}{RT}\right)\rho\right]/\alpha\rho. \tag{21b}$$

We use nonlinear least squares[10] to fit α, b^*, b_1, and b_2, minimizing the difference between $1/G$ found using Eq. (21b) with p-V-T data and $1/G$ computed using p from Eq. (19). Figure 2 shows the final fit with the data of Fig. 1. The factor of 0.25 in Eq. (20), which is absorbed in $\lambda b(T)$, is chosen so that $\lambda\approx0.3$. From Fig. 2 the final value of λ is 0.3159, with the final fit returning $\alpha/v_B=2.145$, $b^*/v_B=1.0823$, $b_1=0.027\,74$ and $b_2=0.235\,78$, where v_B denotes the Boyle volume.[12] These best fit values for α and b^* differ by only 0.2% and 5%, respectively, from simple estimates based on the entropy and free energy of water.[10] Comparing values of Dev in Figs. 1 and 2, where Dev is the root-mean-square (rms) deviation between $1/G$ calculated using Eqs. (21a) and Eq. (21b), shows that the modified equation of state reduces Dev by an order of magnitude compared with the fit using B_2 in Fig. 1.

Figure 3 and Table I show a comparison of densities calculated using the new equation of state [Eq. (19)], the Song and Mason equation of state [Eq. (2)], the Peng Robinson equation of state,[14] and the van der Waals equation of state. For this comparison we used the data of Fig. 1 plus an additional 105 p-V-T measurements of water vapor to cover the range: $80<T<370$ °C, $0.4<p<200$ bar, $0.16<\rho$

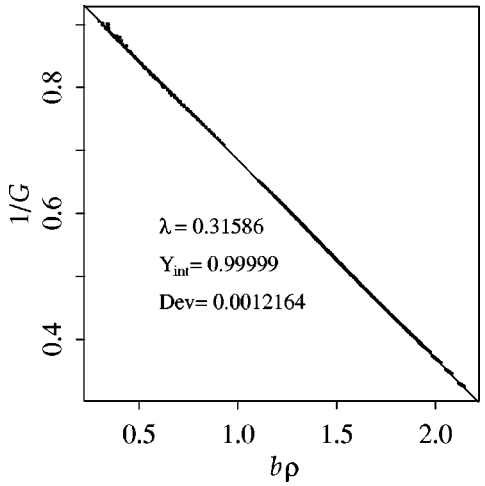

FIG. 2. $1/G$ vs $b\rho$ using Eqs. (18), (19), and the p-V-T data of Fig. 1. Also shown is a best fit straight line with slope λ, y-intercept Y_{int} and rms deviation, Dev.

<145 kg m^{-3}. Tao *et al.*[8] derived a correction term for Eq. (8) that improves the ability of the SMI equation of state for vapour pressures; this correction term, adapted for Eq. (19), is discussed in Appendix A and has been used in Fig. 3 and Table I for both the SMI and the new equation of state. As shown in Table I, the new equation of state is on average 20–30 times more accurate than these other cubic equations of state.

It is more difficult to fit Eq. (21) to p-V-T data that includes either pressures and temperatures above but close to the critical pressure, to high-density data ($\rho>1025$ kg m^{-3}) or to supercooled data. Figure 4 shows the best fit with the addition of data near the critical pressure and temperature (upper left hand corner of the plot), 25 high density data points ($0<T<150$ °C, $300<p<3000$ bar, $1025<\rho<1109$ kg m^{-3}), and 245 supercooled points ($-34<T<0$ °C, $1<p<500$ bar, lower right hand corner of the plot).

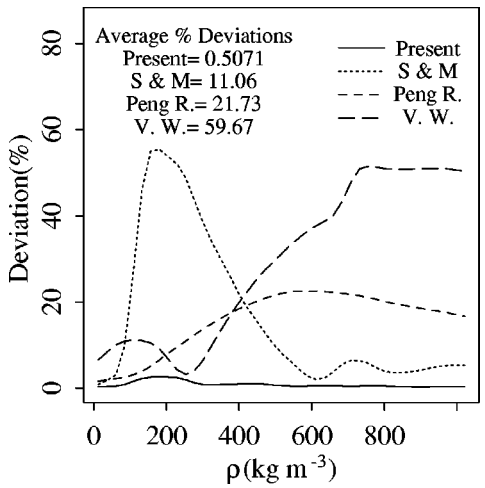

FIG. 3. Comparison of the predictive accuracy of four equations of state. The 1486 p-V-T values are from Haar *et al.* (Ref. 42) in the range $0<T<1200$ °C, $0.1<p<3000$ bar, $0.16<\rho<1025$ kg m^{-3}. Data was binned (bin width=24 kg m^{-3}), and rms percentage deviations of the predicted density calculated and smoothed.

TABLE I. Comparison of the average rms percentage deviation of the predicted density of four equations of state. Data is in the range $0<T<1200$ °C, $0.1<p<3000$ bar, $0.16<\rho<1025$ kg m^{-3}. Note that water vapor data is included but not densities greater than 1025 kg m^{-3}.

	Present	Song & Mason	Peng–Robinson (Ref. 13)	van der Waals
Deviation	0.507	11.06	21.7	59.7

The supercooled data is from Hare and Sorensen[14] and also includes high-pressure p-V-T data produced by integrating Hare and Sorensen's density measurements assuming the speed of sound correlation of Petitet *et al.*[15]

Figure 4 shows a systematic deviation from the law of strong corresponding states at both small and large values of $b\rho$. The supercooled data falls into two clusters in the bottom-right hand corner of the figure. The cluster lying along the best fit line is supercooled data in the region where the density of water anomalously decreases with decreasing temperature. The diverging points above the best fit lines are high-pressure–high-density data in which the density anomaly is suppressed. In Sec. III below we show that the fit in this high $b\rho$ region can be significantly improved by explicitly incorporating strong hydrogen bonds into the equation of state.

III. THE EFFECT OF HYDROGEN BONDS

In the derivation of the present equation of state, hydrogen bonds (HBs) with energy $-a_{VW}\rho$ and entropy $-b^*\rho$ provide the attractive force that holds the fluid together, i.e., at a given temperature and pressure the effect of HBs is to increase the density. Below we will extend the equation of state to describe the behavior of water as it is cooled below 4 °C. When water is cooled below this temperature at atmospheric pressure its density, entropy and internal energy all decrease due to the formation of hydrogen bonds in an open,

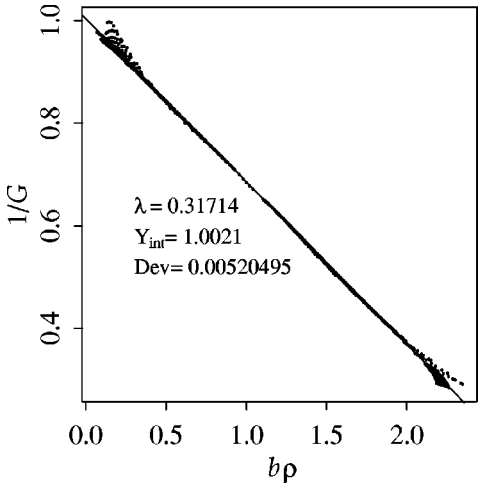

FIG. 4. $1/G$ vs $b\rho$ as in Fig. 2. 1256 p-V-T values are from Haar *et al.* (Ref. 42) in the range $0<T<1200$ °C, $0.1<p<3000$ bar, $100<\rho<1109$ kg m^{-3}. Supercooled data (245 points) is from Hare and Sorensen (Ref. 14) and Petitet *et al.* (Ref. 15) in the range $-34<T<0$ °C, $1<p<500$ bar. The split in the data in the bottom-right corner of the figure is the result of water's density anomaly.

approximately four-coordinated structure.[4] Numerous mixture models have been developed which treat these open tetrahedral HBs as a different species of water that, when formed, can exert their own pressure.[16–18] In this section we adapt a particularly simple mixture model developed by Poole *et al.*[2] to the equation of state presented in Sec. II, and use it to quantitatively predict the thermodynamic properties of water at supercooled temperatures.

A. Free energy of open tetrahedral hydrogen bonds

The effect of hydrogen bonds on the thermodynamic behavior of liquid water can be described by a Helmholtz free energy, A_{HB}, that was approximated by Poole *et al.*[2] using a partition function with two species of HBs

$$A_{\mathrm{HB}} = -fRT\ \ln[\Omega_0 + \exp(-\epsilon_{\mathrm{HB}}/RT)] - (1-f)RT\ \ln(\Omega_0+1), \tag{22}$$

where f is the fraction of HBs that are capable of forming strong (open) bonds with energy, ϵ_{HB}, and Ω_0 is the number of configurations of weak bonds with energy 0. The configuration number, Ω_0, can be written as

$$\Omega_0 = \exp(-S_0/R), \tag{23}$$

where S_0 is the entropy of formation of a mole of weak HBs. Poole *et al.*[2] argued that strong HBs are most likely to occur when the bulk molar volume V is equal to the specific volume of ice I_h (i.e., $V_{\mathrm{HB}} = 1.087\ \mathrm{cm^3\,g^{-1}}$), and therefore, approximated f as

$$f(V) = \exp-[(V-V_{\mathrm{HB}})/\sigma]^2, \tag{24}$$

where the parameter σ characterizes the width of the region surrounding V_{HB} in which strong HBs are able to form.

For their qualitative model Poole *et al.* took S_0 to be the entropy of formation of a mole of strong hydrogen bonds ($-90\ \mathrm{J\,K^{-1}\,mol^{-1}}$), chose a width parameter $\sigma = 0.25 V_{\mathrm{HB}}$, and used the van der Waals equation of state to supply the background attractive force due to closed (nonopen) hydrogen bonds. The contribution of Eq. (22) to the total pressure is therefore

$$p = p_{\mathrm{EOS}} + 2p_{\mathrm{HB}}, \tag{25}$$

where p_{EOS} refers to the pressure calculated using the van der Waals equation of state, and p_{HB} is determined using Eq. (22) and the Maxwell relation

$$p = \left(\frac{\partial A}{\partial V}\right)_T. \tag{26}$$

The factor of 2 in Eq. (25) accounts for the fact there are two moles of HBs for every mole of molecules. As we discuss in Sec. IV, Poole *et al.* showed that with these parameter values and $\epsilon_{\mathrm{HB}} = -22\ \mathrm{kJ\,mol^{-1}}$ (~80% of the HB energy of ice), Eq. (25) produces a second critical point at positive pressure.

B. Adding open hydrogen bonds to the new equation of state

In order to improve the performance at supercooled temperatures of the equation of state described in Sec. II, we will use the approach of Eq. (25) with the following modifications (discussed in greater detail below):

(1) Replace p_{EOS} calculated using the van der Waal equation in Eq. (25) with p_{EOS} given by Eq. (19), using the values for α, and b^* found in Sec. II B 3.
(2) Modify the Poole *et al.* estimates of the energy of strong hydrogen bonds and the entropy of the weak HBs (decreasing $|S_0|$ from 90 $\mathrm{kJ\,mol^{-1}\,K^{-1}}$ to 51 $\mathrm{kJ\,mol^{-1}\,K^{-1}}$ and $|\epsilon_{\mathrm{HB}}|$ from 22 $\mathrm{kJ\,mol^{-1}}$ to $|\epsilon_{\mathrm{HB}}| \approx 13.5\ \mathrm{kJ\,mol^{-1}}$).
(3) Replace the volume dependent expression for the strong hydrogen bond fraction $f(V)$ [Eq. (24)] with a temperature and density dependent expression that falls rapidly to zero at temperatures above 0 °C.
(4) Modify the temperature-dependent excluded volume term $b(T)$ in Eq. (19) to reflect the fact that, as water is cooled below 20 °C, open hydrogen bonds act to decrease the density of the fluid, reducing the need for the excluded volume term $b(T)$ to increase steeply at low temperatures.

Beginning with item 2, we note that the total energy of hydrogen bonds in water, E_{total}, now has two contributions: (i) the van der Waal's free energy $A_{VW} = a_{VW}\rho$ [Eq. (14)], (ii) the bond energy contributed by strong HBs: $E_{\mathrm{HB}} = f\epsilon_{\mathrm{HB}} = A_{\mathrm{HB}} + T\partial A_{\mathrm{HB}}/\partial T$. We estimate A_{VW} at the density of ice to be $\approx -14.2\ \mathrm{kJ\,mol^{-1}}$ (assuming 2 moles of HBs/mole water).[10] If we assume that $f = 1$ at temperatures below the glass transition, where[19] $E_{\mathrm{total}} \approx -28\ \mathrm{kJ\,mol^{-1}}$, then we have $E_{\mathrm{HB}} = E_{\mathrm{total}} - A_{VW} = \epsilon_{\mathrm{HB}} = -13.8\ \mathrm{kJ\,mol^{-1}}$. This value for ϵ_{HB} is close to the measured value of $\epsilon_{\mathrm{HB}} = -13.4\ \mathrm{kJ\,mol^{-1}}$ in supercooled water.[20] We will, therefore, assume that ϵ_{HB} is approximately independent of temperature and density, and that changes in the bond energy E_{total} arise due to the temperature and density dependence of the fraction f of strong hydrogen bonds.

The entropy of the weak HBs, S_0, can also be estimated from simple physical arguments. At 1 bar and 100 °C the entropy of water vapor is 196 $\mathrm{J\,mol^{-1}\,K^{-1}}$. In liquid water at 100 °C the configurational (i.e., total minus vibrational) entropy is about 26% of the total entropy.[21] In water vapor, we would expect this percentage to rise somewhat since the increase in bonded states should be greater than the increase in vibrational states. Therefore, as a lower bound on the magnitude of the entropy we take $|S_0| = 0.26 \times 196\ \mathrm{J\,mol^{-1}\,K^{-1}} = 51\ \mathrm{J\,mol^{-1}\,K^{-1}}$ per mole of water. Note that in water vapor the hydrogen bond interaction is dominated by dimer formation and, therefore, there is one mole of HBs per mole of water molecules.

In addition, we will extend Eq. (22) to include the possibility that there are Ω_{HB} configurations of strong HBs

$$A_{\mathrm{HB}} = -fRT\ \ln[\Omega_0 + \Omega_{\mathrm{HB}}\ \exp(-\epsilon_{\mathrm{HB}}/RT)] - (1-f)RT\ \ln(\Omega_0+\Omega_{\mathrm{HB}}), \tag{27}$$

where

$$\Omega_{\mathrm{HB}} = \exp(-S_{\mathrm{HB}}/R), \tag{28}$$

with $\Omega_{\mathrm{HB}} \ll \Omega_0$.

For item 3, note that the volume dependence of the strong bond fraction f given by Eq. (24) causes f to increase as water is heated beyond its minimum specific volume at 4 °C and atmospheric pressure. To prevent this spurious increase in f we add a steep cutoff above the freezing temperature

$$f(T,\rho) = f^*(\rho) f^{**}(T), \tag{29a}$$

$$f^*(\rho) = \frac{1 + C_1}{\exp[(\rho - \rho_{HB})/\sigma]^2 + C_1}, \tag{29b}$$

$$f^{**}(T) = \exp[-0.18(T/T_f)^8], \tag{29c}$$

where $T_f = 273.15$ K and $0 < C_1 < 1$. The density dependent term, $f^*(\rho)$, is a Gaussian-like function centered around density ρ_{HB} in analogy to Eq. (24), and $f^{**}(T)$ is a low-pass filter centered at T_f. We have switched to density as our dependent variable so that Eq. (29) can be easily included in the equation of state. The modified Gaussian of Eq. (29b) was chosen to produce a more linear dependence of f on density than the Gaussian of Eq. (24).

To estimate σ, we will assume an upper limit of the effect of open HBs at the density of high-density amorphous ice:[22] $\rho = 1.169$ g cm^{-3}. Taking the lower limit of the density of open HBs as the ice density $\rho_i = 0.92$ g cm^{-3}:

$$\begin{aligned} 2\sigma &= 1.169 - 0.92 \ \text{g cm}^{-3}, \\ \sigma &= 0.135\rho_i . \end{aligned} \tag{30}$$

Fitted values for the coefficients C_1 and σ as well as the hydrogen bond density ρ_{HB} will be determined in Sec. III C.

Addressing item 4, we choose a new functional form for the excluded volume term $b(T)$ defined in Eq. (20) that reduces the rise in $b(T)$ at supercooled temperatures

$$b(T)/v_B = 0.2 \exp(-21.4(T/T_B + 0.0445)^3) - b_1 \exp(1.016T/T_B) + b_2, \tag{31}$$

where v_B, T_B are the Boyle volume and temperature and values for the coefficients b_1 and b_2 will be determined in Sec. III C.

C. The final form of the equation of state

In this section we will employ the optimization procedure described in the addendum[10] to determine values for ϵ_{HB}, S_0, S_{HB}, σ, ρ_{HB}, C_1, b_1, b_2 and λ using Eq. (25) with p_{EOS} given by Eq. (19) and $b(T)$ by Eq. (31). We find p_{HB} in Eq. (25) using Eqs. (26) and (27). Values for b^* and α are taken unchanged from Sec. II B 3.

Figure 5 shows the final form of the fit using the data of Fig. 4 excluding 182 data points near the critical point. The addition of p_{HB} has brought the supercooled data in the lower right hand corner of Fig. 4 into better agreement with the law of strong corresponding states, reducing Dev by a factor of 5. The coefficients returned from the fit are:[10]

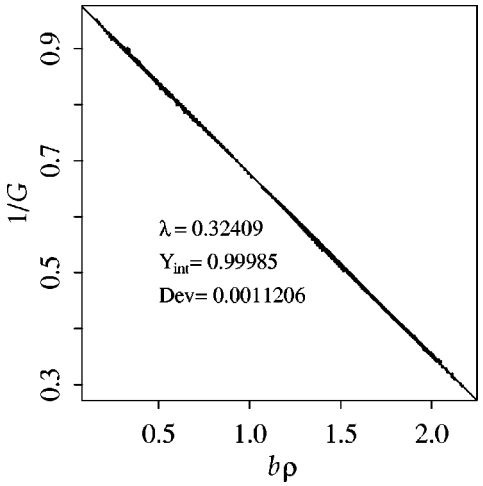

FIG. 5. $1/G$ vs $b\rho$ with the addition of p_{HB}. The p-V-T data (1319 points) is from Fig. 4 excluding 182 points near the critical point. For a fit to an expanded range of p-V-T values that includes higher temperatures and water vapor see Eq. (A1).

$$\begin{aligned} \epsilon_{\mathrm{HB}} &= -11.490 \ \text{kJ mol}^{-1}, \\ S_0 &= -61.468 \ \text{J mol}^{-1}\,\text{K}^{-1}, \\ S_{\mathrm{HB}} &= -5.128 \ \text{J mol}^{-1}\,\text{K}^{-1}, \\ \rho_{\mathrm{HB}} &= 0.8447 \ \text{g cm}^{-3}, \\ C_1 &= 0.7140, \\ \sigma &= 0.1425 \ \text{g cm}^{-3} = 0.1687\rho_{\mathrm{HB}}, \\ b_1 &= 0.250\,81, \\ b_2 &= 0.998\,59, \\ \lambda &= 0.3241. \end{aligned} \tag{32}$$

As in Sec. II B 3, the final values of fitted coefficients such as ϵ_{HB}, S_0, ρ_{HB}, and σ are within 20%–30% of their initial estimated values.

Figure 6 shows the effect of strong hydrogen bonds on the excluded volume term $b(T)$. The solid line labeled b(12,6) is taken from Tao *et al.*[8] and is appropriate for nonpolar fluids. This can be compared with the two versions of $b(T)$ given by Eq. (20) (dotted line, labeled ''b'') and Eq. (20) (dashed line, labeled ''b with p_{HB}''). The inclusion of p_{HB} produces a less rapid increase in $b(T)$ at lower temperatures because the anomalous decrease in density at supercooled temperatures can be fit instead by the p_{HB} term in Eq. (25).

Densities generated by Eq. (25) at pressures between 1 and 2800 bar are shown in Fig. 7. The inset shows the removal of the density maximum as the pressure is increased from 800 to 1200 bar. At low temperatures and pressures, the formation of open HBs forces a local density commensurate with their perfect tetrahedral geometry. As a result the density of water decreases with decreasing temperature. At higher pressures, the pressure breaks the perfect geometry of the HBs and the density maximum is absent.

The removal of the density maximum with increasing pressure can also be seen in Fig. 8, which shows isotherms

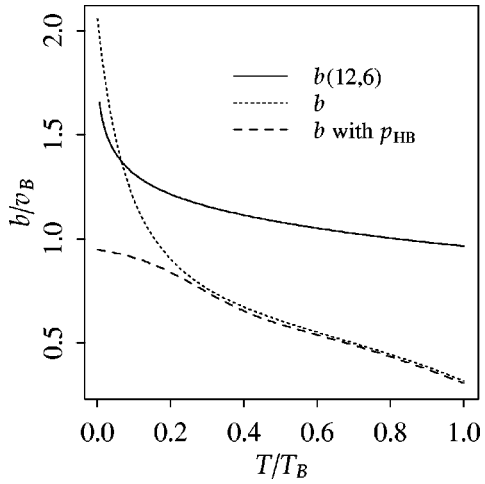

FIG. 6. Comparison of the excluded volume b as a function of the temperature normalized by the Boyle temperature T_B. Solid line: b computed by Tao *et al.* (Ref. 8) for a (12,6) potential. Dotted line: Eq. (30) with coefficients determined by fitting Eq. (18) with the data of Fig. 2. Dashed line: Eq. (30) with coefficients determined by fitting the equation of state with the hydrogen bond term to the data of Fig. 4.

between -40 °C and 500 °C. Above ≈850 bar the supercooled isotherm (-40 °C) is denser than the 0 °C isotherm. However, at low pressures, the supercooled isotherm crosses the 0 °C isotherm and becomes less dense. This behavior is consistent with the experimental evidence that the temperature of the density maximum is displaced to lower temperatures by increasing pressure.[23] Further discussion of the performance of the equation of state with and without hydrogen bonds is given in the addendum.[10]

The free energy A, entropy S, and heat capacity C_p can also be obtained from Eq. (25) using Eq. (26) and the Maxwell relations

$$S=-\left(\frac{\partial A}{\partial T}\right)_\rho, \quad C_p=T\left(\frac{\partial S}{\partial T}\right)_P. \tag{33}$$

In Appendix B we derive expressions for A for the equation of state with and without strong hydrogen bonds, using Eq. (33) to obtain the heat capacity for pressures between 1 and 800 bar and temperatures between -35 °C and 800 °C. As we show in Appendix B the equation of state reproduces both the anomalous increase in heat capacity at 1 bar and low temperatures and the decrease in heat capacity below 0 °C at higher pressures.

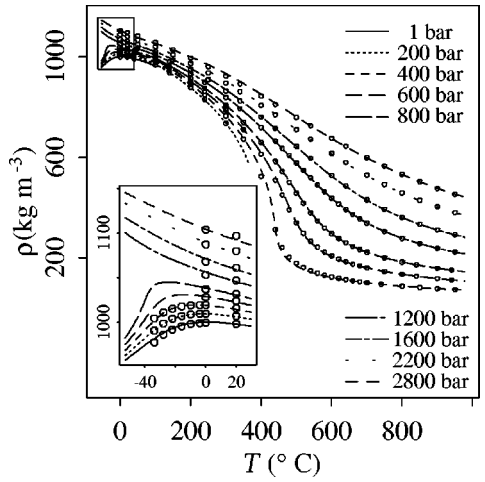

FIG. 7. Isobaric density. ○ from Haar *et al.* (Ref. 42), Hare and Sorensen (Ref. 14) and Petitet *et al.* (Ref. 15).

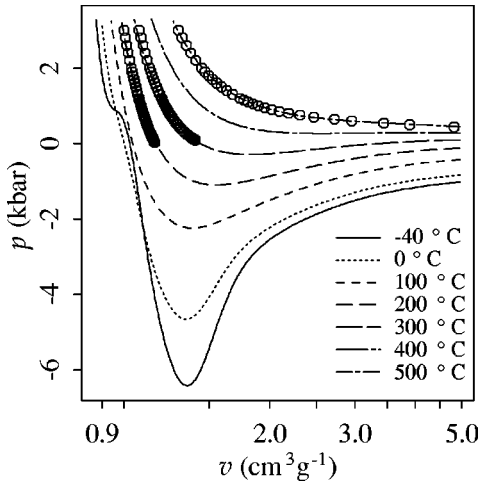

FIG. 8. Isotherms showing the suppression of the density maximum at higher pressures. ○ from Haar *et al.* (Ref. 42).

In the next section we examine the behavior of the equation of state at low temperatures in the metastable region of the phase diagram.

IV. THE THERMODYNAMIC BEHAVIOR OF WATER AT LOW TEMPERATURES

In Sec. III and Appendix A we added open hydrogen bonds to the modified SMI equation of state, showing that it can accurately reproduce the observed thermodynamic behavior of water over a wide range of temperatures and pressures. In this section we will examine the behavior of the equation of state at low temperatures for which the liquid phase is metastable and, therefore, inaccessible to observation. Central to the prediction of the thermodynamic behavior of water at these temperatures is the behavior of the vapor–liquid spinodal,[24] $P_s(T)$, defined as the locus of isochore minima satisfying

$$\left(\frac{\partial P}{\partial T}\right)=0. \tag{34}$$

The behavior of $P_s(T)$ is closely related to the question of whether water has a second critical point. One proposal, first suggested by Speedy and Angell,[25] is the ''stability limit conjecture,''[26,27] which postulates that in the p,T plane the spinodal is ''reentrant,'' tracing a continuous curve from the critical temperature and pressure to negative pressures, where it reaches a minimum before returning to positive pressures at supercooled temperatures.[24]

More recently, Poole *et al.*[24,28] have proposed that the phase diagram of water contains a new liquid–liquid spinodal terminating in a second critical point. This new spinodal defines an area in which two forms of supercooled water exist: Low-density water (LDW) and high-density water (HDW). Thus in this theory the vapour–liquid spinodal is divergent, as is the case for a simple van der Waals liquid.

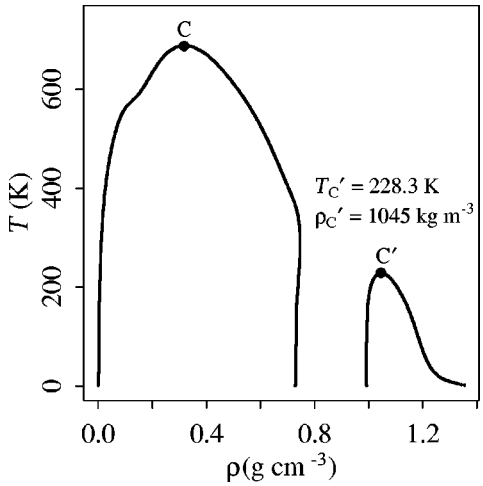

FIG. 9. The vapor–liquid spinodal terminating at a critical point C, and the LDW–HDW spinodal terminating at a second critical point C'.

Because of the absence of a stability limit for supercooled water, there is a continuity of states between liquid and solid water.

The Poole *et al.*[2] mixture model described in Sec. III A can produce either a reentrant spinodal, given $|\epsilon_{HB}| = 14$ kJ mol^{-1}, or a second liquid–liquid spinodal, given $|\epsilon_{HB}| = 22$ kJ mol^{-1}. In Figs. 9 and 10 we show the spinodals for the new equation of state, calculated using the coefficient values of Eq. (32) and Appendix A. Even though the best-fit $|\epsilon_{HB}| = 11.5$ kJ mol^{-1} for the new equation of state is smaller than Poole's 14 or 22 kJ mol^{-1}, the new equation of state produces a second LDW–HDW spinodal with a critical point at $T_c = 228$ K, $p_c = 954$ bar. Figure 10 is very similar to the phase diagram proposed by Poole *et al.*[29] and Stanley *et al.*,[30] with the exception of the termination of the liquid–liquid spinodal at much larger positive and negative pressures (not shown). There have been a wide range of other estimates for the values of the critical parameters for a liquid–liquid spinodal. Some of these are listed in Table II, including the recent estimate of Mishima and Stanley[31] based on measurements of decompression-induced melting of ice IV.

TABLE II. Comparison of the critical parameters of a second critical point in water generated from the present equation of state with the estimations of other authors.

	$p_{C'}$ (kbar)	$\rho_{C'}$ (g cm^{-3})	$T_{C'}$ (K)
Present	0.954	1.045	228.3
Stanley *et al.* (Ref. 30)	1.2	⋯	185
Ponyatovskiĭ *et al.* (Ref. 46)	0.33	⋯	225
Tanaka (Ref. 33)	−1.0	⋯	240
Sciortino *et al.* (Fig. 12) (Ref. 35)	⋯	1.08	180
Sciortino *et al.* (Fig. 13) (Ref. 35)	1.2	⋯	200
Mishima and Stanley (Ref. 31)	1	⋯	220

The equilibrium line separating HDW and LDW is also shown on Fig. 10 (short-dashed line). It is natural to associate HDW, which lies to the left of the equilibrium line, with high-entropy–high-density amorphous-solid water (called Water II by Speedy[32]). Speedy[32] showed that Water II, obtained by vapor deposition between 136 and 150 K, cannot be connected to supercooled liquid water at 236 K by a thermodynamically continuous and reversible path. This is also true of HDW for the new equation of state. Figure 10 shows that HDW heated at atmospheric pressure from 150 K intersects the HDW–LDW spinodal at 167 K without crossing the equilibrium curve, and thus is not connected to LDW by a continuous path. The instability limit of 167 K predicted by the new equation of state is very close to the 170 K instability limit estimated by Speedy.[32] Figure 10 demonstrates that a thermodynamically self-consistent phase diagram of water is possible without moving the critical point to negative pressures as suggested by Tanaka.[33]

The temperature of maximum density (TMD) line shown on Fig. 10 consists of the locus of points for which the density given by the new equation of state is maximum. Figure 12 shows that, at positive pressures, the TMD line terminates at a spinodal as predicted by Speedy.[26] The new equation of

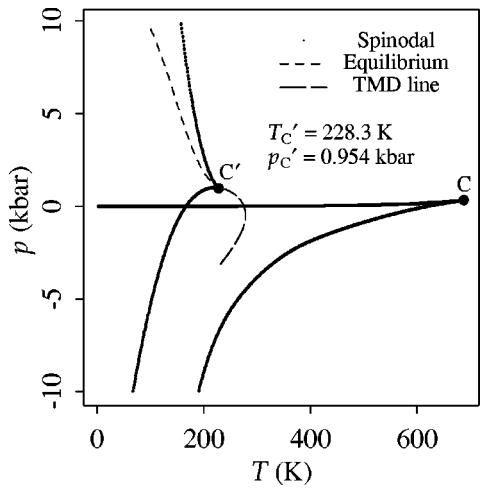

FIG. 10. Same as Fig. 9. Also shown are the equilibrium line and the TMD line.

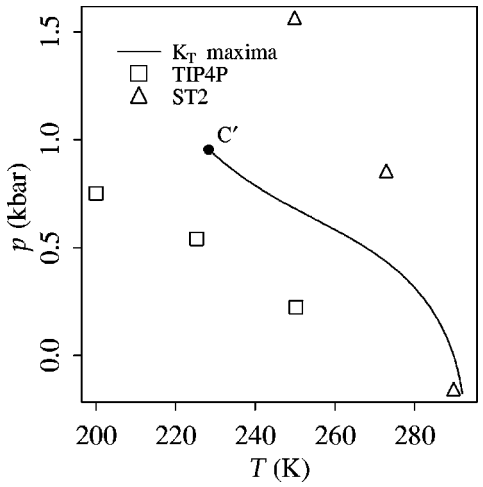

FIG. 11. Comparison of isothermal compressibility (K_T) maxima between the new equation of state of water, and the ST2 and TIP4P potentials (Ref. 35). The line of K_T maxima exhibits a smooth transition from ST2 like behavior near $p = 0$ kbar to TIP4P behavior at higher pressures, ending in a second critical point (C').

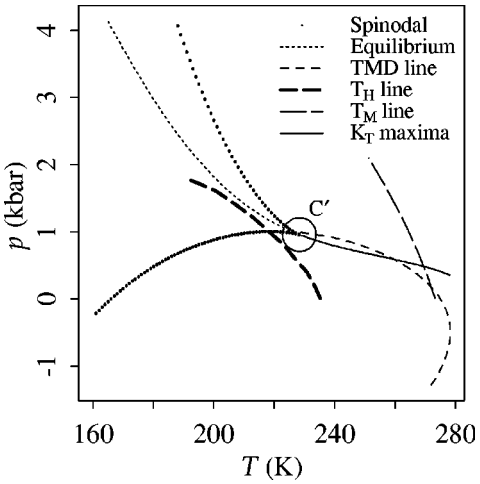

FIG. 12. The phase diagram of the new equation of state of water. The liquid–liquid spinodal terminates at a second critical point at C' (circled). The temperature of maximum density (TMD) line intersects the LDW spinodal just above C'. At negative pressures the TMD line decreases with decreasing pressure. Also shown are the K_T maxima from Fig. 11. The melting temperature (T_M) line is from Wagner *et al.* (Ref. 36). The homogeneous freezing temperature (T_H) line (Ref. 37) resembles the HDW $\leftrightarrow$ LDW equilibrium transition line above $\approx$1.2 kbar. It is suggested that a first-order HDW$\rightarrow$LDW phase transition may determine T_H at high pressures.

state gives a TMD at atmospheric pressure of 1.5 °C, 2.5 K less than the experimentally measured maximum. This can be contrasted with the TMD calculated from molecular-dynamics simulations using the ST2 and TIP4P interparticle potentials.[24] The TIP4P potential produces a TMD in the vicinity of 260 K, which is ~17 K below the experimental TMD at atmospheric pressure.[24] Thus the thermodynamic anomalies predicted by TIP4P are somewhat weaker than in real water. The ST2 potential, on the other hand, exhibits a TMD ~35 K above the experimental TMD, and therefore, overestimates the thermodynamic anomalies of water.[24] The strong anomalous behavior of ST2 is attributed to the fact that ST2 overemphasizes the tetrahedral character of the *H*-bonding groups on the water molecule.[24]

Another thermodynamic parameter that can be calculated from the equation of state is the locus of isothermal compressibility (K_T) maxima in the (p,T) plane. Sastry *et al.*[34] have shown that this $K_T^{\max}$ line is useful in characterizing the critical behavior of different numerical and analytical models of water. Sciortino *et al.*[35] have compared the K_T maxima produced by molecular-dynamics simulations using the ST2 and TIP4P potentials and found that ST2 produces maxima that increase quickly with decreasing temperature, terminating in a second critical point near $p=2$ kbar, $T=240$ K. For TIP4P, the magnitude of the maxima is significantly smaller than for ST2 and Sciortino *et al.*[35] were unable to determine if the line does, in fact, terminate in a second critical point.

Figure 11 compares $K_T^{\max}$ calculated using the new equation of state and the ST2 and TIP4P potentials. The $K_T^{\max}$ line for the equation of state lies between those calculated for ST2 and TIP4P, which is consistent with the TMD behavior discussed above. At low pressures (low densities) the hydrogen bond term p_{HB} in Eq. (25) acts as a repulsive force trying to force a density commensurate with an open tetrahedral hydrogen bond formation. Thus the behavior of $K_T^{\max}$ near $p=0$ kbar is similar to that produced by the ST2 potential. As the pressure increases, the effect of p_{HB} is reduced with increasing density [cf. Eq. (29b)], and the behavior of $K_T^{\max}$ is similar to that found using the TIP4P potential.

Figure 12 shows an expanded view of the liquid–liquid spinodal, TMD line, equilibrium line, and $K_T^{\max}$ line calculated by the equation of state. We have also added two sets of observations: The melting line from Wagner *et al.*[36] and homogeneous freezing temperatures (T_H) measured by Kanno *et al.*[37] Figure 12 shows that at the pressure of the second critical point (1 kbar), $T_H=218$ K, 10 degrees lower than T_c. This implies that this region of the phase diagram may be experimentally accessible. Figure 12 also shows that at 1.2 kbar the homogeneous freezing temperature is nearly coincident with the HDW–LDW equilibrium curve, suggesting that T_H may be determined by a phase transition from high-density (high-entropy) liquid water to low-density (high-entropy) liquid water at these high pressures. The increasing divergence of T_H and the equilibrium line as temperature decreases is consistent with an increase in the hysteresis of this first-order phase transition as the self-diffusivity decreases. A phase transition would cause immediate nucleation because of the sudden decrease in the ice–water surface energy which according to a relation by Turnbull[38] is proportional to the latent heat of melting. A discontinuity in the experimentally measured T_H or in the statistics of the homogeneous nucleation process (i.e., volume dependence, mean time before nucleation, etc.), if found, would provide evidence in support of the liquid–liquid spinodal predicted by the new equation of state. Elsewhere we discuss in more detail the use of the new equation of state to calculate homogeneous nucleation rates for supercooled water.[39,40]

V. SUMMARY

We have developed a new analytic equation of state for water that is accurate over a wide range of pressures (0.1$\rightarrow$3000 bar) and temperatures (−34$\rightarrow$1200 °C), including the supercooled region. It consists of three parts: (i) A modified form of the SMI equation of state that is accurate for liquid water in the p-ρ-T range $0.1<p<1200$ bar, $0<T<700$ °C, $250<\rho<1015$ kg m^{-3}; (ii) A correction term based on a proposal by Tao and Mason[8] that improves the ability of the equation of state to predict vapor pressures; (iii) A term representing the contribution of open hydrogen bonds to the free energy of the fluid, based on the approach of Poole *et al.*[2]

The attractive forces for the equation of state are modeled by hydrogen bonds that contribute both internal energy and entropy terms to the total free energy of water. Consistent with current theories of liquids[6] the attractive forces are assumed to make only a first-order contribution to the virial expansion. The repulsive forces are modeled using the strong principle of corresponding states developed by Ihm *et al.*,[3] with the temperature dependence of the repulsive force fit using p-V-T data for water. We are able to make accurate

initial guesses for the fitted coefficients using hydrogen bond energy and entropy data.

We argue in Sec. III that the energy of strong hydrogen bonds, ϵ_{HB}, should be ~ -13.5 kJ mol^{-1} a value that is close to the optimal value returned by fitting the equation of state to p-V-T data that includes supercooled measurements. We followed Poole *et al.* in introducing these open tetrahedral bonds into the equation of state using a simplified partition function, which we modified to include a temperature dependence that suppressed open HB formation above the melting line. The resulting equation of state quantitatively reproduces all of the observed anomalous behavior of supercooled water including: (i) A density maximum near 0 °C at 1 bar that is suppressed to lower temperatures with increasing pressure; (ii) the anomalous increase in heat capacity at 1 bar and low temperatures; (iii) a decrease in heat capacity below 0 °C at higher pressures. The melting point is accurately predicted at atmospheric pressure.

The new equation of state also predicts a liquid–liquid spinodal and a second critical point at positive pressure. The absence of a re-entrant spinodal is consistent with experimental evidence that supercooled water does not approach the limit of stability upon cooling at atmospheric pressure.[41] The locus of maxima of the isothermal compressibility lies between that predicted by molecular-dynamics simulations using the TIP4P and ST2 potentials.

We also find that the equilibrium line between high-density and low-density liquid water coincides closely to the measured homogeneous freezing temperature at pressures above 1.2 kbar. If the equilibrium line predicted by the equation of state is accurate, we would expect that the nucleation rate of rapidly supercooled droplets at pressures above 1.2 kbar is controlled by phase change, and is independent of droplet size and cooling rate. Such nucleation observations would provide useful information on the low-temperature properties of liquid water.

ACKNOWLEDGMENTS

We are grateful to Marcia Baker for introducing us to Poole *et al.*[2] and to Marcia and Birger Bergersen for many helpful discussions. We also thank an anonymous reviewer for comments that improved the manuscript. This work is supported by grants from the Atmospheric Environment Service and the National Science and Engineering Research Council of Canada.

APPENDIX A: VAPOR CORRECTION TERM

Tao and Mason[8] improved the ability of the original SMI equation of state [Eq. (8)] to predict vapor pressures by including a correction term, I_1

$$p = p_{EOS} + I_1 \rho^2 RT, \tag{A1}$$

where p_{EOS} is given by Eq. (8) an I_1 is given by

$$I_1 \approx (\alpha - B_2)\chi(\rho,T) \approx (\alpha - B)\xi(T)\phi(\rho), \tag{A2}$$

with

$$\xi(T) = A_1(e^{\kappa T_C/T} - A_2), \tag{A3}$$

$$\phi(\rho) = \frac{b\rho}{1 + 1.8(b\rho)^4}. \tag{A4}$$

Tao and Mason also related the constants A_1, A_2, and κ to the Pitzer acentric factor, ω, as follows:

$$A_1 = 0.143,$$
$$A_2 = 1.64 + 2.65[\exp(\kappa - 1.093) - 1], \tag{A5}$$
$$\kappa = 1.093 + 0.26[(\omega + 0.002)^{1/2} + 4.50(\omega + 0.002)].$$

The resulting equation for I_1 is, therefore

$$I_1 = A_1(\alpha - B_2)b\rho \frac{(e^{\kappa T_C/T} - A_2)}{1 + 1.8(b\rho)^4}. \tag{A6}$$

To apply a correction of the form of Eq. (A2) to the present equation of state, we modify $\phi(\rho)$ and $\xi(T)$ to limit their range of influence. The dense gas region of the p-V-T surface is already well fit, so we want an expression for $\phi(\rho)$ that decreases rapidly at high densities, and an expression for $\xi(T)$ that decreases rapidly above the critical temperature. We also want both expressions to be bounded as $T \to 0$ K so that we can examine the low-temperature behavior of the equation of state in Sec. IV.

Versions of $\phi(\rho)$ and $\xi(T)$ that have the necessary temperature and density dependence are

$$\phi(\rho) \approx \frac{\exp[A_4(\rho/\rho_c)^{6.9}]}{1 + A_3(\rho/\rho_c)^{3.3}} \quad \text{without } p_{HB}, \tag{A7a}$$

$$\phi(\rho) \approx \frac{\exp[A_4(\rho/\rho_c)^{6.7}]}{1 + A_3(\rho/\rho_c)^{3.2}} \quad \text{with } p_{HB}, \tag{A7b}$$

and

$$\xi(T) = A_1 \exp[-A_5(T/T_C)^6] \frac{(T - \kappa T_C)^2 + A_2}{T_C^2}, \tag{A8}$$

where $\kappa \approx 1$. Like Tao and Mason's temperature dependence, this expression increases as the temperature decreases, but unlike Tao and Mason's it decreases rapidly to zero above the critical temperature.

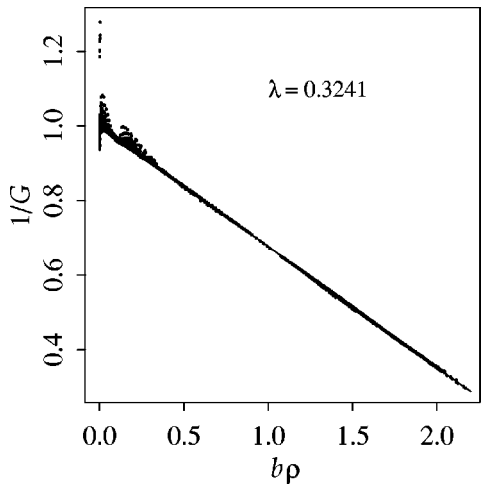

FIG. 13. $1/G$ vs $b\rho$ using Eq. (18) which includes the hydrogen bond term p_{HB} and the vapor correction term I_1 [Eq. (A2)]. Liquid data is the same as Fig. 4 and water vapor has also been added from Haar *et al.* (Ref. 42). A total of 1785 p-V-T points were used.

We have used two version of $\phi(\rho)$ because we want to include a vapor correction term to the equation of state both with and without p_{HB}. Determination of the coefficients $A_1 - A_6$ and κ is done by refitting the appropriate equation [Eq. (18) or (24)] to data that now includes 105 vapor measurements in the range $80<T<370$ °C, $0.4<p<200$ bar, $0.16<\rho<145$ kg m^{-3}. Only the coefficients A_1-A_6 and κ are varied, the other coefficients are fixed to the values determined in Sec. II B 3 and Eq. (32). Figure 13 shows the final form of the fit for the full equation of state with both the p_{HB} and I_1 terms. As expected, the inclusion of I_1 has a negligible affect on the ability of the new equation of state to collapse liquid densities to a line.

The values for the coefficients returned by the fit are

without pHB	with pHB
$A_1=-12.12$	$A_1=-12.16$
$A_2=2.294\times10^4$	$A_2=2.284\times10^4$
$A_3=13.60$	$A_3=13.33$
$A_4=0.0527$	$A_4=0.0610$
$A_5=1.8784$	$A_5=1.873$
$\kappa=0.8368$	$\kappa=0.8366.$

APPENDIX B: FREE ENERGY AND HEAT CAPACITY OF LIQUID WATER

We can determine the entropy S and heat capacity C_p of liquid water using the analytic equation of state (without the vapor correction term) and the Maxwell relations Eqs. (25) and (32). Integrating the pressure to obtain the free energy via Eq. (25) produces an undetermined function of temperature, $\psi(T)$ which we find by fitting the free energy predicted by the equation of state to measurements. In Sec. B 1 below we find an analytic expression for $\psi(T)$ for the equation of state without the p_{HB} term. Adding the p_{HB} term to the equation of state produces a nonintegrable expression for the entropy; in Sec. B 2 we estimate the resulting $\psi(T)$ as a residual and show the resulting C_P.

1. Free energy without p_{HB}

The Helmholtz free energy ignoring hydrogen bonds, A_{EOS} follows from integration of Eq. (25) using Eq. (18)

$$\begin{aligned} A_{\mathrm{EOS}} &= A_{\text{ideal gas}} \\ &\quad + \int_0^{\rho}\left(-RTb^*\rho^2 - a_{VW}\rho^2 + \frac{RT\alpha\rho^2}{1-\lambda b\rho}\right)\frac{d\rho}{\rho^2} \\ &= RT\,\log\rho - RTb^*\rho - a_{VW}\rho - \frac{RT\alpha}{\lambda b}\log(1-\lambda b\rho) \\ &\quad - RT(\log\Lambda^{-3}+1) - RT\psi(T) + A_0 \\ &= A_1(\rho,T) - RT\psi(T), \end{aligned} \tag{B1}$$

where Λ is the thermal wavelength in molar units given by

$$\Lambda = \sqrt{\frac{R^{5/3}h^2}{2\pi m K_B^{8/3} T}}, \tag{B2}$$

$\psi(T)$ is an undetermined nondimensional function of temperature, and A_0 is a constant of integration.

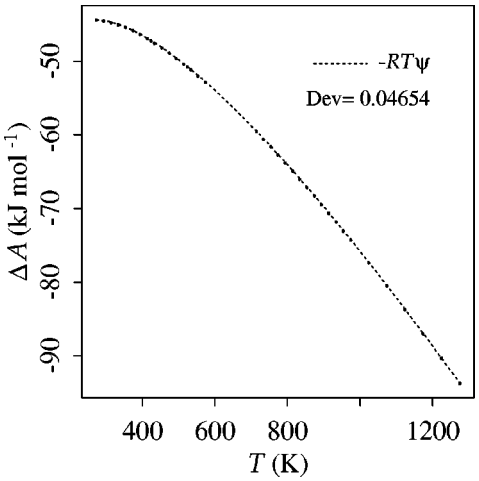

FIG. 14. $-RT\psi$ vs T calculated from Eq. (B3) along with rms deviation, Dev. The points are calculated from Eq. (B1) and data from Haar *et al.* (Ref. 42) assuming $S_0=63.34$ J mol^{-1} K^{-1} and $U_0=-42.9$ kJ mol^{-1} at the triple point.

We approximate the undetermined function $\psi(T)$ as a smooth function of the non-dimensional parameters T_B/T and $(\lambda b)/\alpha$, where λ, α and $b(T)$ have values determined in Sec. II B 3

$$\psi(T) = \psi_1 + \psi_2\frac{T_B}{T}\frac{\lambda b}{\alpha} + \psi_3\frac{T}{T_B}. \tag{B3}$$

Free energy data (A_{meas}) from Haar *et al.*[41] was used to determine the coefficients of $\psi(T)$ and A_0 in Eq. (B1) by minimizing the difference $A_{\mathrm{meas}}-A_{\mathrm{EOS}}$. The optimal fitted constants are found to be $A_0=21.47$ kJ mol^{-1} and $(\psi_1,\psi_2,\psi_3)=$ (5.13, 20.04, and 2.73), respectively.

We plot the fitted function $-RT\psi(T)=A_{\mathrm{EOS}}-A_1$ in Fig. 14. For comparison we have included the measurements, plotted as $\psi_{\mathrm{meas}}=A_{\mathrm{meas}}-A_1$. The absolute entropy, S_0, and internal energy, U_0, at the triple point were also needed in the calculation of A_{meas}. They were calculated from Cox

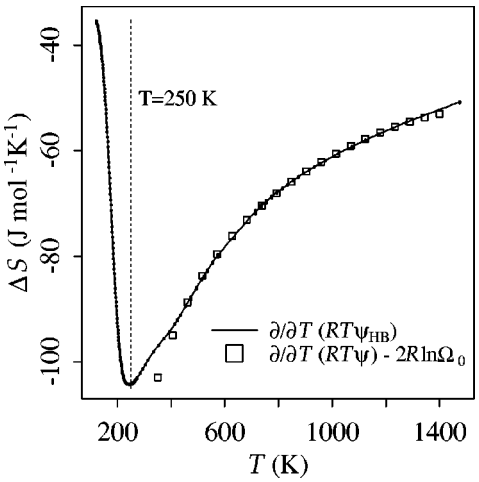

FIG. 15. Plot of $\partial/\partial T(RT\psi_{\mathrm{HB}})$ obtained through Eq. (B4) as described in Section B 2. The points are obtained from the entropy data of Haar *et al.* (Ref. 42) and from the integrated C_p data of Angell (Ref. 44). For comparison, $\partial/\partial T(RT\psi)-2R\ln\Omega_0$ where ψ is given by Eq. (B3) is also shown.

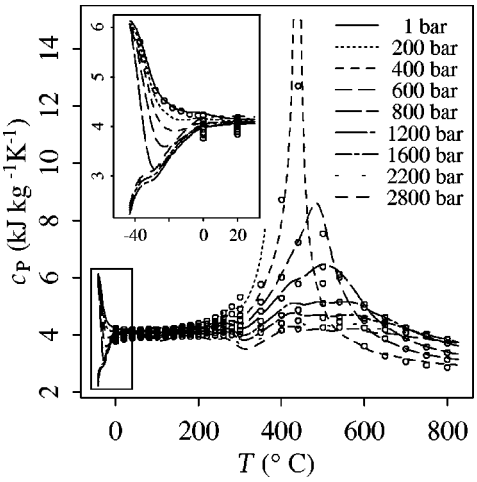

FIG. 16. Isobaric heat capacity, C_p. ○ from Haar *et al.* (Ref. 42) and Angell (Ref. 44). Note: C_p at 400 bar has been limited to 15 kJ kg^{-1} K^{-1}.

et al.[43] and were estimated as $S_0=63.34$ J mol^{-1} K^{-1} and $U_0=-42.9$ kJ mol^{-1} taking the enthalpy of water[19] to be -56 kJ mol^{-1}.

2. Free energy and C_p with p_{HB}

The addition of the open hydrogen bond term p_{HB} to the equation of state produces a more complex expression for A_{EOS} that is no longer a function of only the dimensionless parameters, T/T_B and $(\lambda b)/\alpha$. We will determine the new form of $\psi(T)$ using entropy data that extends to supercooled temperatures. The corresponding expression for the entropy from the equation of state, S_{EOS} is

$$S_{\mathrm{EOS}}=-\frac{\partial A_1}{\partial T}+\frac{\partial RT\psi_{HB}(T)}{\partial T}-2\frac{\partial A_{HB}}{\partial T}, \tag{B4}$$

where A_1 is given by Eq. (B1) and A_{HB} by Eq. (26).

We find the term $\partial(RT\psi_{HB})/\partial T$ as the residual $\Delta S=S_{\mathrm{meas}}+\partial(A_1+2A_{HB})/\partial T$ where S_{meas} consists of our integration of the supercooled heat capacity measurements of Angell[44] and entropy data from Haar *et al.*[42] For temperatures below the glass transition temperature ($T=136$ K) we take S_{meas} to be the entropy of ice, while between 136 and 231 K S_{meas} is joined by a smooth curve to Angell's integrated values.

Figure 15 shows a third-order polynomial fit of the residual $\Delta S=\partial(RT\psi_{\mathrm{HB}})/\partial T$. Also shown (small dots) are the measurements used in the fit. To the left of the dotted vertical line at $T=250$ K is the extrapolation of $\partial(RT\psi_{\mathrm{HB}})/\partial T$ to the glass transition at 136 K. For comparison we show as square boxes the values for $\partial(RT\psi)/\partial T-2R\ln\Omega_0$ calculated using the $\psi(T)$ found in Sec. B 1. To permit direct comparison of Eqs. (B3) and (B4) we have added $-2R\ln\Omega_0$, which is $2\partial A_{\mathrm{HB}}/\partial T$ in the limit $f\to 0$, to $\partial(RT\psi)/\partial T$ given by Eq. (B3).

Figure 16 shows heat capacities found using Eqs. (B4) and (32) with $\psi(T)$ determined by numerical integration of the polynomial fit. The increase in C_p near the critical temperature and pressure and the increase in the supercooled region are both produced. The anomalous C_p maximum of about 6.15 J mol^{-1} K^{-1} at 1 bar is consistent with a continuous transition of states from supercooled water to ice.

Although determining $\psi(T)$ numerically prohibits us from extrapolating S_{EOS} to the deeply supercooled part of the phase diagram, we note that the sharp increase in C_p seen in Fig. 16 is due to the hydrogen bond term A_{HB}, and not to the fitted function $\psi_{\mathrm{HB}}(T)$. Negative values of $\partial(RT\psi_{\mathrm{HB}})/\partial T$ act through Eq. (32) to decrease, not increase, the heat capacity.

[1] C. H. Cho, S. Singh, and G. W. Robinson, Phys. Rev. Lett. **76**, 1651 (1996).
[2] P. H. Poole, F. Sciortino, T. Grande, H. E. Stanley, and C. A. Angell, Phys. Rev. Lett. **73**, 1632 (1994).
[3] G. Ihm, Y. Song, and E. Mason, J. Chem. Phys. **94**, 3839 (1991).
[4] We follow Poole *et al.* (Ref. 2) in using the term ''open hydrogen bonds'' to denote strong hydrogen bonds formed among water molecules in an approximately tetrahedral structure, similar to the open lattice of ice I_h.
[5] Y. Song and E. A. Mason, Phys. Rev. A **42**, 4749 (1990).
[6] Y. Song and E. Mason, J. Chem. Phys. **91**, 7840 (1989).
[7] D. A. McQuarrie, *Statistical Mechanics* (Harper & Row, New York, 1976).
[8] F. Tao and E. Mason, J. Chem. Phys. **100**, 9075 (1994).
[9] J. D. Weeks, D. Chandler, and H. C. Andersen, J. Chem. Phys. **54**, 5237 (1971).
[10] See AIP Document No. E-PAPS: E-JCPSA6-110-527901 for Postscript and PDF versions of this appendix and supporting documentation (computer programs to calculate density and entropy). E-PAPS document files may be retrieved free of charge from the FTP server (http://www.aip.org/epaps/epaps.html) or from ftp.aip.org in the directory /epaps/. For further information: e-mail: paps@aip.org or fax: 516-576-2223.
[11] $T_c=647.3$ K, $p_C=2.205\times10^7$ Pa.
[12] Using the expression for B_2 from Hill and MacMillan (Ref. 44) gives $T_B=1408.4$K, $v_B=4.1782\times10^{-5}$ m^{-3} mole^{-1}.
[13] G. A. Melhem, R. Saini, and B. M. Goodwin, Fluid Phase Equilibria **47**, 189 (1989).
[14] D. E. Hare and C. M. Sorensen, J. Chem. Phys. **87**, 4840 (1987).
[15] J. P. Petitet, R. Tufeu, and B. L. Neindre, Int. J. Thermophys. **4**, 35 (1983).
[16] M. Vedamuthu, S. Singh, and G. W. Robinson, J. Phys. Chem. **98**, 2222 (1994).
[17] M. Vedamuthu, S. Singh, and G. W. Robinson, J. Phys. Chem. **99**, 9263 (1995).
[18] R. L. Lamanna, M. Delmelle, and S. Cannistraro, Phys. Rev. E **49**, 2841 (1994).
[19] D. Eisenberg and W. Kauzmann, *The Structure and Properites of Water* (Claredon, Oxford, United Kingdom, 1969).
[20] S. Chen, in *Hydrogen-Bonded Liquids*, edited by J. C. Dore and J. Teixeira (Kluwer Academic, Hingham, Massachusetts, 1991).
[21] M. G. Sceats and S. A. Rice, in *Water, A Comprehensive Treatise*, edited by F. Franks (Plenum, New York, 1982), Vol. 7, Chap. 2.
[22] O. Mishima, L. D. Calvet, and E. Whalley, Nature (London) **310**, 393 (1984).
[23] C. A. Angell, in *Water, A Comprehensive Treatise*, edited by F. Franks (Plenum, New York, 1982), Vol. 7, Chap. 1.
[24] P. H. Poole, F. Sciortino, U. Essmann, and H. E. Stanley, Phys. Rev. E **48**, 3799 (1993).
[25] R. J. Speedy and C. A. Angell, J. Chem. Phys. **65**, 851 (1976).
[26] R. J. Speedy, J. Phys. Chem. **86**, 982 (1982).
[27] R. J. Speedy, J. Phys. Chem. **86**, 3002 (1982).
[28] P. H. Poole, U. Essmann, F. Sciortino, and H. E. Stanley, Phys. Rev. E **48**, 4605 (1993).
[29] P. H. Poole, U. Essmann, F. Sciortino, and H. E. Stanley, Nature (London) **360**, 324 (1992).
[30] H. E. Stanley, C. A. Angell, U. Essmann, M. Hemmati, P. H. Poole, and F. Sciortino, Physica A **205**, 122 (1994).
[31] O. Mishima and H. E. Stanley, Nature (London) **392**, 164 (1998).
[32] R. J. Speedy, J. Phys. Chem. **96**, 2322 (1992).
[33] H. Tanaka, J. Chem. Phys. **105**, 5099 (1996).
[34] S. Sastry, P. G. Debenedetti, F. Sciortino, and H. E. Stanley, Phys. Rev. E **53**, 6144 (1996).

[35] F. Sciortino, P. H. Poole, U. Essmann, and H. E. Stanley, Phys. Rev. E **55**, 727 (1997).
[36] W. Wagner, A. Saul, and A. Pruss, J. Phys. Chem. Ref. Data **23**, 515 (1994).
[37] H. Kanno, R. J. Speedy, and C. A. Angell, Science **189**, 880 (1975).
[38] D. Turnbull, J. Appl. Phys. **21**, 1022 (1950).
[39] C. A. Jeffery and P. H. Austin, J. Geophys. Res. **102**, 25269 (1997).
[40] C. A. Jeffery, Master's thesis, University of British Columbia, 1996, p. 106.
[41] Y. Xie, K. F. L. Jr., and G. Morales, Phys. Rev. Lett. **71**, 2050 (1993).
[42] L. Haar, J. S. Gallagher, and G. Kell, *NBS/NRC Steam Tables* (Hemisphere, New York, 1984).
[43] J. D. Cox, D. D. Wagman, and V. A. Medvedev, *Codata Key Values for Thermodynamics* (Hemisphere, New York, 1989).
[44] C. A. Angell, M. Oguni, and W. J. Sichina, J. Phys. Chem. **86**, 998 (1982).
[45] P. G. Hill and R. D. C. MacMillan, Ind. Eng. Chem. Res. **27**, 874 (1988).
[46] E. G. Ponyatovskiĭ, V. V. Sinand, and T. A. Pozdnyakova, JETP Lett. **60**, 360 (1994).